Measurement of the coagulation rate constant for sulfuric acid particles as a function of particle size using tandem differential mobility analysis

Tak Wai Chan, Michael Mozurkewich*

Department of Chemistry and Centre for Atmospheric Chemistry, York University, 4700 Keele Street, Toronto, Canada ON M3J 1P3

Abstract

A new method for the determination of coagulation rate constants for monodisperse, neutral particles is described. In this method, a differential mobility analyzer (DMA) is used to prepare a monodisperse aerosol and a second DMA is used to separate the coagulation products from the original monodisperse particles. The experiments are carried out under initial rate conditions so that typically 5–9% of the monomer particles undergo coagulation. Experimental results at 298 ± 1 K for H_2SO_4/H_2O particles with diameters of 49–127 nm and a composition of 72–73% H_2SO_4 by mass gave enhancement factors, relative to rate constants calculated for hard spheres, that vary from about 1.2 for the largest particles to 2.8 for the smallest particles. Fitting these results to a theoretical expression accounting for van der Waals forces gives a Hamaker constant of $(6.4 \pm 2.6) \times 10^{-13}$ erg. We also give convenient formulas for computing coagulation enhancement factors from the Hamaker constant.

1. Introduction

Sulfuric acid aerosol is the ultimate product of the oxidation of anthropogenic sulfur dioxide and naturally emitted reduced sulfur compounds such as dimethylsulfide. Although the atmospheric aerosol is very complex, H_2SO_4 and H_2O are usually the major components. In particular, it is often assumed that particles formed by homogenous nucleation in the atmosphere initially consist

* Corresponding author. Tel.: + 1-416-736-5246; fax: + 1-416-736-5936.
E-mail address: mozurkew@yorku.ca (M. Mozurkewich).

entirely of H_2SO_4 and H_2O. The processes by which these particles form and grow are still poorly understood. But these processes are important since they affect the number concentration and size distribution of the atmospheric aerosol which, in turn, have direct and indirect influences on climate (Twomey, 1991; Preining, 1991; Leaitch, Isaac, Strapp, Banic & Wiefe, 1992; Schwartz, 1996; Saxena & Menon, 1999). One significant part of these processes is growth by coagulation.

Intermolecular attractions (dispersion or van der Waals' forces) produce an increase in coagulation rate constants for particles in the free molecular and transition regimes (Schmidt-Ott & Burtscher, 1982; Alam, 1987; Huang, Seinfeld & Marlow, 1990). This increase is often expressed in terms of the enhancement factor, defined as the ratio of the experimental coagulation rate constant to the value predicted by hard sphere collision theory; the enhancement factor is always greater than unity.

Experimental results give a variety of results for enhancement factors. Fuchs and Stugin (1965) reported enhancement factors of 2.8 and 2.3 for NaCl particles with diameters of 5 and 9 nm, respectively. For these particles, they estimated a somewhat smaller theoretical enhancement factor of 2.2. Mercer and Tillery (1971) studied the coagulation rates of room air particles produced by radon decay, their results indicated that the enhancement factor is about 4. Shon, Kasper and Shaw (1980) studied NaCl particles with diameters of 18–105 nm and reported that the enhancement factor is no larger than 1.1 even for the smallest particles. Okuyama, Kousaka and Hajashi (1984) measured coagulation rates for 5–40 nm diameter particles of various compositions. They obtained enhancement factors of about 2 for NaCl, from 1 to 3 for $ZnCl_2$ and between 5 and 10 for Ag. These values were somewhat smaller than the theoretically expected values for $ZnCl_2$ and NaCl and much larger than expected for Ag. McMurry (1980) simulated the evolution of the size distribution of photochemically generated H_2O–H_2SO_4 aerosols in a smog chamber and reported that using an enhancement factor of 1.98 gave generally better agreement than neglecting van der Waals forces. Brockmann, McMurry and Liu (1982) studied coagulation of ammonium sulfate particles and found an enhancement factor of about 2.1 over the diameter range of 5–40 nm. Theory (Sceats, 1989) predicts a substantial variation in enhancement factor over the size ranges covered in the experiments of McMurry and Brockmann et al., Van Dingenen and Raes (1990) reported enhancement factors for H_2O–H_2SO_4 aerosols that increased from 1.2 for diameters of about 200 nm to 2.0 for diameters of about 30 nm.

The above results clearly cover a wide range and provide little information on the size dependence of the enhancement factor in the transition regime. Here we describe a new method for the determination of coagulation rate constants for monodisperse, neutral particles. The method is an adoption of the TDMA technique (Rader & McMurry, 1986); it uses a differential mobility analyzer (DMA) to produce a monodisperse aerosol (Knutson & Whitby, 1975; Pui & Kinney, 1991) and a second DMA to separate the coagulation products from the original aerosol. This allows us to vary the particle size over a reasonable range in the transition regime. A key aspect of this approach is that we measure the initial rate of formation of the coagulation products rather than the rate of disappearance of the total particle number. This makes the method much more sensitive and much less subject to errors caused by deposition of particles in the apparatus. We use the method to determine coagulation rate constants as a function of particle size for H_2O–H_2SO_4 aerosols. The results are compared to theoretical calculations to determine the Hamaker constant for these particles.

2. Experimental

2.1. Apparatus

A flow diagram of the experimental set up is shown in Fig. 1. Clean, dry air was supplied by an Aadco 737 pure air generator. The air flows were controlled by calibrated MKS 1259C mass flow controllers. Sulfuric acid aerosol was generated by mixing SO_3(g) with humid air in a 1/8 in. stainless-steel tee. SO_3(g) was produced by bubbling 10–50 sccm (standard cm^3 per minute) of air through a glass frit immersed in fuming sulfuric acid (19–24% SO_3 by mass); the bubbler was kept in a constant temperature bath at 20.2°C. An air flow of 1000–2000 sccm was humidified by passing a portion of the flow through a humidifier consisting of a 100 cm length of Nafion tubing (permeable to water but not air) immersed in distilled water. After mixing this saturated portion of the flow with the dry portion, the humidity was monitored by a humidity sensor (Vaisala Humitter 50U). For the experiments described here, the humidity at this point was kept at 40 ± 1%, except for a few experiments in which it was kept at 60 ± 1%.

Once the SO_3 and H_2O flows were mixed, the aerosol was allowed to pass through a 220 cm^3 tubular chamber; this allowed the aerosol to grow by coagulation. It was found that the stability of the aerosol number concentration was improved by using a circulating water bath to keep the chamber at 20.2°C. The size of the particles exiting the chamber could be altered by changing either the air flow through the chamber or the air flow that was saturated with SO_3. Using a faster flow through the chamber, or a smaller SO_3 flow, produced smaller particles while a slower total flow or a larger SO_3 flow produced larger particles.

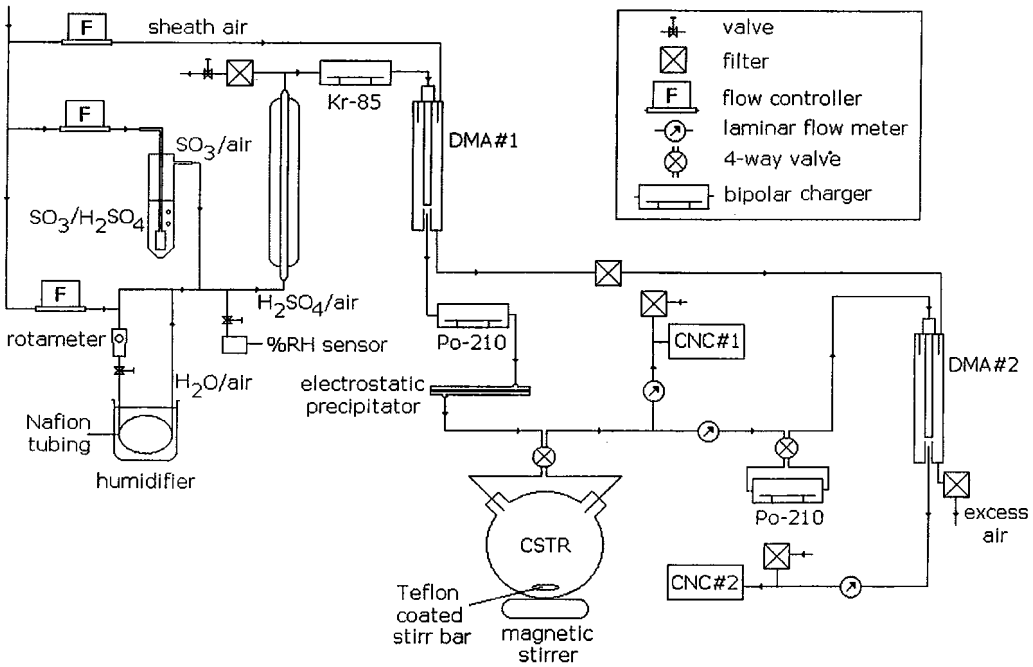

Fig. 1. Flow diagram of the experimental apparatus.

A portion of the polydisperse aerosol exiting the chamber was charged by a ^{85}Kr bipolar charger and a monodisperse fraction was obtained by using a TSI 3071 differential mobility analyzer (DMA#1) set at an appropriate voltage. The aerosol inlet and outlet flows of DMA#1 were maintained at 483 accm (actual cm^3 per minute). All aerosol flows in this experiment were monitored using the pressure drop across laminar flow elements which were calibrated against the mass flow controllers. The sheath air flow was 6000 sccm. Since the sheath air was dry, the relative humidity of the aerosol leaving the DMA was much lower than that of the aerosol entering the DMA.

The charge on the monodisperse aerosol was removed by passing the aerosol through a ^{210}Po bipolar charger and then through an electrostatic precipitator. The precipitator consisted of a 26 cm length of 1/2 in.o.d. stainless-steel tube with a 1/8 in.o.d. stainless-steel rod passed through the center. The rod was typically held at 1800 V. The efficiency of the electrostatic precipitator was tested before each experiment by bypassing the bipolar charger on DMA#2 and confirming that no particles were detected at the outlet of DMA#2 for any appropriate voltages.

Coagulation of the monodisperse aerosol occurred inside a continuously stirred tank reactor (CSTR). This consisted of a three necked, round bottom, glass flask with an estimated volume of 5.2 l. A four-port valve was used to either direct the aerosol flow through the CSTR or to bypass the CSTR while adjusting the experimental conditions. The CSTR contained a 1.5×6 cm Teflon-coated stirring bar driven by a magnetic stirrer; this was used to maintain homogeneous conditions in the CSTR. The data analysis is based on the assumption that the CSTR was well mixed; however, too large a stirring rate results in excessive deposition of particle on the walls. An insufficient stirring rate could be detected by the fact that it resulted in substantial fluctuations in number concentration while the CSTR was being filled. For these experiments, the stirring rate was adjusted so that while filling the CSTR the root-mean-square fluctuation in the number density was less than 1% (compared to 10% without stirring) while giving a steady-state number density within 1% of that obtained without stirring. An estimation of the stirring rate used during the experiment was about 140–150 rpm. The residence time in the CSTR was approximately 650 s.

The temperature in the CSTR was monitored using a Hg in glass thermometer inserted into the CSTR. The temperature inside the CSTR was typically 25 ± 1°C. Over the course of an experiment (approximately one and a half to two hours) this temperature varied by 0.5 to 1°C. This slight temperature fluctuation is not big enough to significantly affect either the coagulation rate or the residence time in the reactor.

The total number density of particles exiting the reactor was monitored by withdrawing a flow of 150 accm to a TSI 7610 condensation nuclear counter (CNC#1). After passing through a laminar flow element the flow was diluted with clean air to provide the total flow ($\sim$1500 accm) required by the CNC.

The remainder of the flow could be either sent on to the second DMA or diverted to a cooled mirror dewpoint hygrometer (EG&G model 911, not shown in Fig. 1) to determine the relative humidity of the aerosol flow. Except when checking the dewpoint, this flow passed through a second ^{210}Po bipolar charger and a second differential mobility analyzer (DMA#2). The sheath air for DMA#2 was the filtered excess air from DMA#1. The aerosol flows were maintained at 333 accm. Filtered room air was added to the aerosol flow exiting DMA#2 to provide the total flow required by CNC#2 (TSI model 7610). A computer data acquisition system was used to operate DMA#2 in fast scan mode (Wang & Flagan, 1990) and to record the counts from both

CNCs. Each data set consists of about 80–100 scans depending on the length of the experiment. Each scan from DMA#2 took 90 s and consisted of 45 mobility bins with voltages ranging from one-half to three times the voltage set on DMA#1. The first 6 points of each scan were not used since steady state was not yet established in the DMA. The size resolution of the distribution measured with DMA#2 was sufficient to allow the concentrations of the initial particles (monomers) and coagulation products (dimers) to be determined separately.

2.2. Procedure

All experiments were carried out in a dynamic mode in which the concentrations of monomers and dimers were measured as conditions inside the CSTR changed in response to changes in the aerosol entering the CSTR. The rate equations were then fit to the concentrations in order to determine coagulation and wall loss rate constants. The data analysis procedure requires that the concentrations be known as functions of the time in the CSTR. However, since the particles take time to pass through the connecting tubing, the bipolar charger, and DMA#2, there is a difference between the time at which the number concentration is measured at CNC#2 and the time at which that concentration was present in the CSTR. This time delay was measured as part of the procedure.

Prior to beginning an experiment, the four-port valve was set so that the flow bypassed the CSTR. The operating conditions were adjusted to provide a reasonable number of particles of the desired size and the voltage on DMA#2 was adjusted to match the maximum of the distribution leaving DMA#1. The voltage on DMA#1 was then set to zero to provide particle-free air and the flow was directed through the CSTR which was thoroughly flushed out. While clean air was passing through the reactor, the flow was briefly diverted to the dew point hygrometer so that the relative humidity inside the reactor could be determined.

When the voltage on DMA#1 was turned on, the particle number concentration in the CSTR started to increase as particle-free air was replaced with the aerosol. We refer to this as filling the CSTR. During the first 180 s of filling (the first two scans of DMA#2), the voltage on DMA#2 was kept constant at the maximum of the distribution leaving DMA#1; the data taken during this interval were used to determine the delay time as discussed below. DMA#2 was then changed to scanning mode and used to determine the size distributions. The total number concentration exiting the reactor was monitored by CNC#1.

After approximately 90–100 min, the monomer and dimer concentrations reached constant, steady-state values. The voltage on DMA#1 was then set to zero so that no fresh monomer was introduced into the CSTR. The particle concentrations then decreased as the aerosol was replaced by clean air. We refer to this as flushing the CSTR. Data collected during flushing was especially useful in determining the wall loss rate constants for the monomer and dimer.

The time delay, Δt_2 defined as the time required for particles to flow from the CSTR to CNC#2, was determined as follows. Let t_1 be the flow time from DMA#1 to the CSTR and let t_2 be the flow time from DMA#1 to CNC#2, then

$$\Delta t_2 = t_2 - t_1. \tag{1}$$

During the first 180 s of filling, the concentrations measured by CNC#1 and CNC#2 were recorded and plotted as functions of time. These plots gave straight lines with intercepts at $t_1 + \Delta t_1$

and t_2, respectively, where Δt_1 is defined as the time required for particles to flow from the CSTR to CNC#1. Δt_1 is much smaller than the other quantities; by using the tubing volumes and flow rates it was estimated to be 3.0 ± 0.5 s. Then t_1 and t_2 were obtained from the intercepts and substituted in Eq. (1) to obtain the time delay, Δt_2. The average delay was found to be 38.9 ± 4.4 s; this was reasonably consistent with the value estimated from the volumes and flow rates. The average value for t_1 was 18.5 ± 4.2 s. The error limits for t_1 and t_2 are the standard deviations of the means of the values obtained for all experiments.

2.3. Particle composition

In most of these experiments, particle-free air from DMA#1 was continuously flowed through the CSTR between experiments. When this was done with the humidifier kept at 40% RH, the measured dewpoints in the air exiting the CSTR were -24 ± 1°C. This corresponds to relative humidities in the CSTR of 2.8 ± 0.4%. The corresponding equilibrium composition of the particles, calculated using the tables of Gmitro and Vermeulen (1964), was 72.5 ± 0.5 wt% H_2SO_4. Experiments with the humidifier at 60% RH gave dewpoints of -21.9%°C, CSTR relative humidities of 3.4%, and particle compositions of 71.7% H_2SO_4. In some of the early experiments, the flow was allowed to bypass the CSTR between experiments. In these experiments, the dew points were initially very high and only slowly reached a constant value as air flowed through the CSTR; this was due to water vapor infiltrating the CSTR between experiments. Subsequent outgassing of water from the CSTR walls raised the dewpoints. For these experiments the measured dewpoints were -23.5 ± 1°C, the relative humidities were 3.0 ± 0.3%, and the H_2SO_4 weight percentage in the aerosol was 72.2 ± 0.5%.

3. Data reduction

3.1. Fitting of size distributions

Typical size distributions for the aerosol exiting the CSTR are shown in Fig. 2. There are three peaks. One, centered at approximately the voltage set on DMA#1, corresponds to the monomer. The peak at twice this voltage consists of larger particles ($2V$ particles) that were doubly charged when passing through DMA#1 but singly charged at DMA#2. These $2V$ particles have a minor effect in the data analysis. The middle peak corresponds to particles with twice the volume of the monomer; these are the dimers produced by coagulation. From the two sets of data in Fig. 2, it can be clearly seen that, as the experiment proceeds, the concentration of dimer increases more rapidly than that of the monomer.

Since the three peaks partially overlap, it was necessary to fit all three simultaneously. This was done by generating a synthetic distribution function including a Gaussian instrumental spreading function (Stolzenburg & McMurry, 1988). Non-linear regression was used to adjust the parameters of the function to produce the best fit to the measured data. There were seven parameters in the fit: a single instrumental spreading parameter, the standard deviation of the spreading function and, for each of the three peaks, both a number concentration and a centroid voltage offset. The voltage offset was required because the peaks were not quite in their expected positions. This was due to

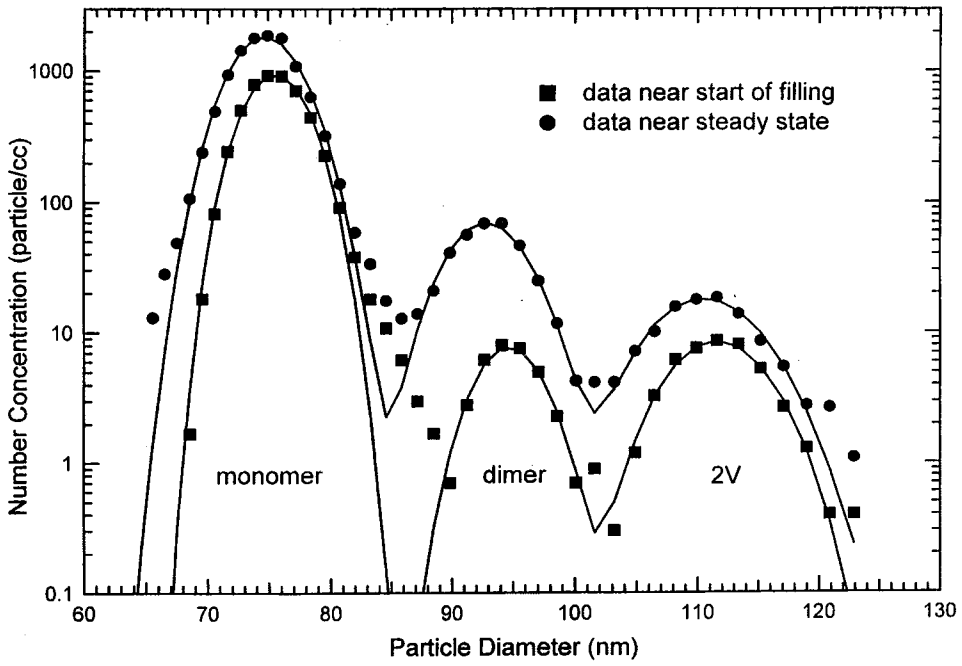

Fig. 2. Typical size distributions exiting the CSTR in the filling and steady-state case. The points are measured concentrations and the lines are best fits.

both a slight systematic difference between the two DMAs and a small amount of evaporation that caused the particles to decrease slightly in size during the course of an experiment. The monomer diameter typically decreased by 1.1–2.2 nm (1.2–3.7%) during filling, remained constant at steady state, and decreased by 5.5–8.5 nm (6.3–19.5%) during flushing. In general, larger diameter changes were observed when smaller size particles were used. The relatively large decrease during flushing was due to the fact that there was no replacement of the particles by fresh particles during this portion of the experiment. Since the coagulation rate constant were primarily determined by the data obtained at steady state, the average size at steady state was taken as the size for which the rate constant was measured. Although evaporation of the particles occurred throughout the experiment, it did not affect the number concentration being measured.

The synthetic distribution was generated by separately calculating the distribution for each of the three peaks and then combining the three distributions. For the monomer and $2V$ particles, the distributions were calculated by convolving the theoretical transfer functions for the two DMAs operating at the measured flow rates and then applying a Gaussian instrumental spreading function. For the dimer peak, the shape was computed by numerically coagulating the theoretical monomer distribution exiting DMA#1 and then applying the transfer function for DMA#2 and the instrumental spreading function.

The fits in Fig. 2 show a slight systematic deviation on the high-voltage sides of the peaks. Although the cause of this has not been identified, we suspect that it is due either to non-ideal performance of the DMAs or to the implicit assumption of plug flow in the calculation of the distribution. The deviation does not significantly affect the results; it is only visible because of the

logarithmic scale used in Fig. 2. The standard deviation of the instrumental spreading function was typically about 3% during filling, remained constant during steady state, and then increased slightly during the flushing case. For the smallest particles, the spreading factor increased to as much as 6–10% during flushing. This can be attributed to the partial evaporation of the particles. Individual particles experienced a spread of residence times in the CSTR and therefore evaporated to varying degrees; this produced an increase in the width of the distribution. The spread in residence times increased during filling, remained constant during steady state, and then increased again during flushing. Since the small particles evaporated to a greater degree, a larger increase in the spreading function was observed for the smaller particles. This made it difficult to carry out experiments for particles with diameters of less than 60 nm since the spreading of the monomer and $2V$ peaks tended to obscure the dimer peak.

The uncertainties in reading the aerosol flows measured by the laminar flow meters on DMA#2 were estimated to be $\pm$ 4%. Due to their effect on the DMA transfer function, these each give an error of 1.9% in the particle concentration. The aerosol flow exiting DMA#2 is also used in determining particle concentration from the count rate measured by CNC#2; thus, the flow uncertainty leads to a random error (between experiments) in the particle concentrations of 6.2%. Since this error will have the same effect on both the monomer and dimer concentrations, this source of error leads to an uncertainty in individual coagulation rate constants of 6.2%. We estimate that the corresponding systematic error in the flows and the rate constants is less than 2%.

3.2. *Charging fraction*

The number concentrations resulting from the fits of the distribution functions are those of the fraction of the particles bearing a single positive charge. The charging fractions for the ^{210}Po bipolar charger was determined as follows. With the aerosol bypassing the CSTR, a monodisperse aerosol was generated with DMA#1 at voltage V. The charge on the aerosol was removed by passing it through a bipolar charger and the electrostatic precipitator. Then, the aerosol was passed through a second bipolar charger, and the size distribution was measured with DMA#2. The scans with DMA#2 covered a sufficient range to include the peaks at $V/2$ and $2V$ that result from particles that were doubly charged at DMA#2 and DMA#1, respectively. Because of the relatively narrow size distribution and small median diameter from the SO_3 source, larger charge multiples were unimportant. The aerosol number densities were kept low enough that the number of dimer particles formed by coagulation was not significant compared to the three peaks (at V, $V/2$, and $2V$) that were being measured.

Let the number concentrations in these three peaks be $N_{V/2}$, N_V, and N_{2V}. Then we have

$$N_{V/2} = Af_2, \tag{2}$$

$$N_V = Af_1 + A'f'_2, \tag{3}$$

$$N_{2V} = A'f'_1, \tag{4}$$

where A and A' are the number concentrations of the monomer (singly charged in DMA#1) and $2V$ (doubly charged in DMA#1) particles that exit from precipitator, f_1 and f_2 are the fractions of the monomer that are singly and doubly charged by the ^{210}Po charger for DMA#2, and f'_1 and

f'_2 are the fractions of the $2V$ particles that are singly and doubly charged at DMA#2. The total number density of particles that enter the bipolar charger for DMA#2 is monitored by CNC#1, let this be N_T, given by

$$N_T = A + A'. \tag{5}$$

Eqs. (2)–(5) are four equations with six unknowns. To circumvent this, the charge fraction measurements were started by setting the voltage of DMA#1 to a value where A' was negligible so that Eqs. (2)–(5) could be solved for f_1 and f_2. The voltage on DMA#1 was then reduced by half so that the values of f_1 and f_2 from the previous voltage became f'_1 and f'_2 at the new voltage. Then new values of f_1 and f_2 were determined and the process was repeated to obtain the charging fractions for a sequence of sizes. A number of such sequences were obtained using various initial voltages.

As noted above, the uncertainties in $N_{V/2}$, N_V, and N_{2V} are about 5%. The estimated uncertainty in N_T was about 2%. Propagating these uncertainties through the procedure described above leads to an uncertainty of about 5.6% for the largest particles increasing to 7.5% for smaller particles. These uncertainties were used to weight the data in determining best-fit polynomials.

Fig. 3 shows the experimental charging fraction as a function of particle size along with the best-fit polynomials. For the singly charged fraction, the results were fit to a third-order polynomial whereas the results for the doubly charged fraction were fit to a second-order polynomial. The scatter about these curves is consistent with the estimated uncertainties in the data points. The estimated uncertainty in the charging fractions calculated from these polynomials is about 3.5%. In combination with the estimated errors from the DMA flows, we get an estimated 'between experiments' uncertainty of 7.4% in determining the monomer and dimer concentrations.

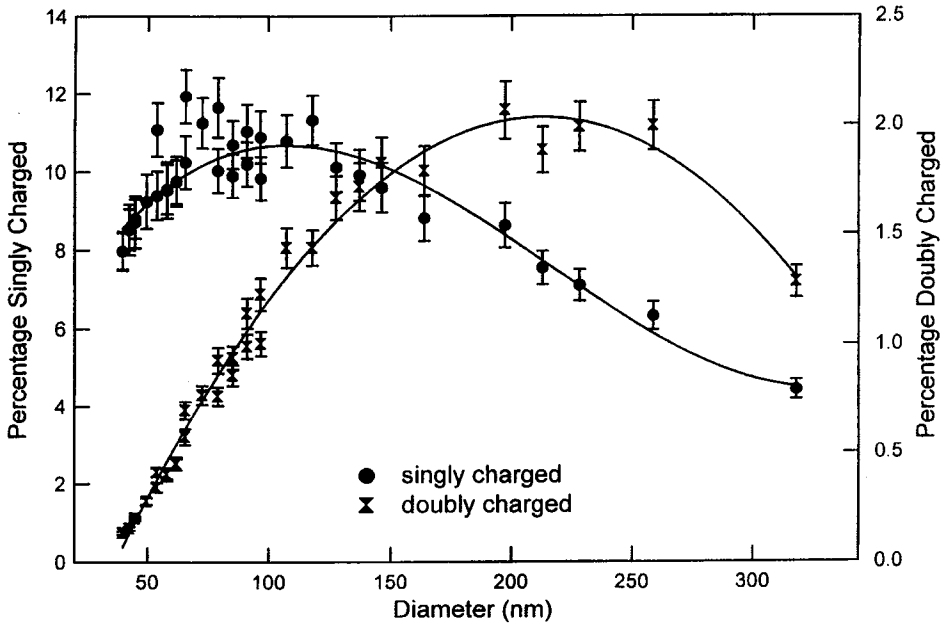

Fig. 3. Charging efficiency of the ^{210}Po bipolar charger for singly and doubly charged particles. Points are measured efficiencies, lines are best-fit polynomials.

As a check on the accuracy of the number concentrations, we computed the ratio of the total of the three peaks measured by DMA#2 to the total measured by CNC#1. The former total included a small correction for the production, via coagulation, of larger particles. The average of these ratios was 0.97 with a standard deviation of 0.14. Although the average is in reasonable agreement with the expected ratio of unity, the standard deviation is nearly double that expected from the estimated uncertainties in the number concentrations. This discrepancy is largely due to three outliers; the most severe of these gave a 37% difference between the two methods of measuring the total number.

The obtained charge distributions were compared with the charge distributions calculated using the theory of Fuchs (Wiedensohler, 1988). The singly charged distribution obtained in this study follows a trend similar to the calculated distribution, but with about half the magnitude of the calculated values. The doubly charged distribution goes through a maximum at about 200 nm, unlike the calculated distribution. The magnitudes for the calculated doubly charged fractions are about 5–11 times the observed values.

3.3. Fitting the number concentration

The raw number concentrations resulting from the fits of the distributions were corrected using the charging fractions determined as described above. The concentration in the $2V$ peak was used to correct the monomer concentration for $2V$ particles that were doubly charged at DMA#2. Fig. 4 shows a typical plot of the monomer and dimer number concentrations as functions of time

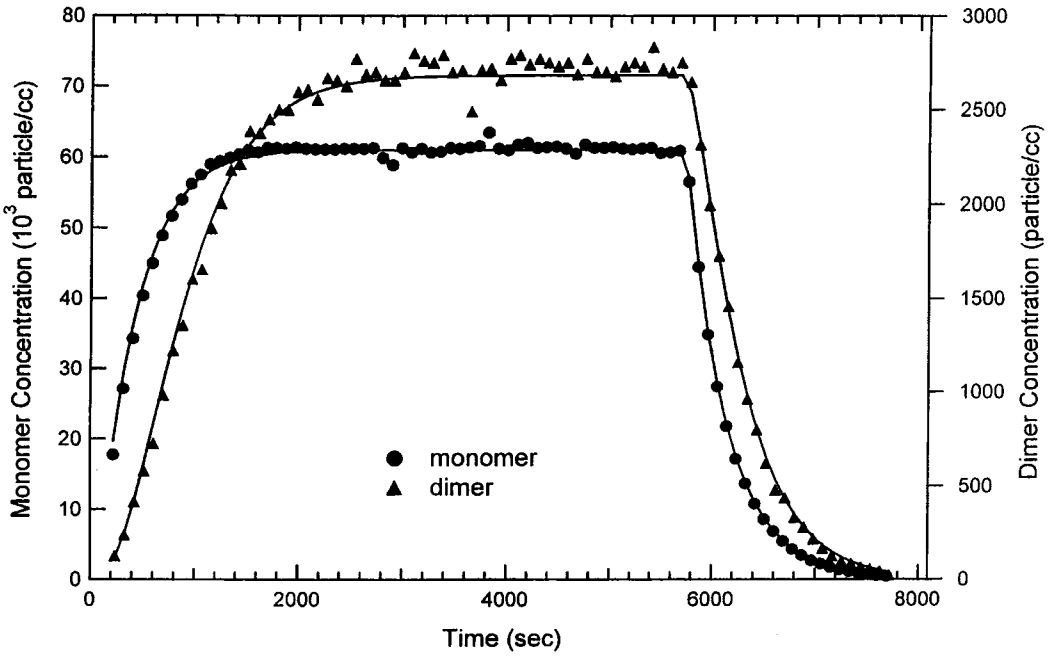

Fig. 4. Typical time trace of monomer and dimer concentrations. Points are measured concentrations, corrected for charging fraction, and lines are best fits to the kinetic model. The voltage on DMA#1 was turned off at 5691 s.

as the CSTR is filled and flushed. The sole source of monomer to the CSTR is the flow into the CSTR. If the concentration of monomer entering the CSTR is $[M]_0$ then the source rate per unit volume is $k_F[M]_0$ where k_F is the flushing rate constant defined by $k_F = Q/V$, V is the volume of the CSTR and Q is the volumetric flow rate. The major processes that remove the monomer are flow out of the reactor with rate constant k_F and coagulation to form dimer

$$M + M \rightarrow D \tag{6}$$

with rate constant k_C. Minor removal processes are deposition on the walls of the CSTR with rate constant k_W and coagulation of monomer with dimer

$$M + D \rightarrow P \tag{7}$$

with the $2V$ particles

$$M + L \rightarrow P \tag{8}$$

and with coagulation products larger than the dimer,

$$M + P \rightarrow P. \tag{9}$$

Since these latter processes are all very minor and should have similar rate constants they are given a common rate constant k'_C. All coagulation rate constants here are written as for coagulation between identical particles. These processes give the following rate equation for the monomer:

$$\frac{d[M]}{dt} = k_F[M]_0 - \{k_F + k_W + 2k_c[M] + 2k'_c([D] + [L] + [P])\}[M]. \tag{10}$$

The dimer is produced by coagulation in the CSTR and by flow into the CSTR. Although the dimer concentration exiting DMA # 1 should be zero, some dimer will be produced by coagulation while flowing from DMA # 1 to the CSTR; this requires a time Δt_1 determined as described in the procedure section above. If it is assumed that the changing charge state of the aerosol in this region does not affect the coagulation rate constant, then the concentration of dimer entering the reactor, $[D]_0$, should be $k_C[M]^2\Delta t_1$. We found that using this value of $[D]_0$ or allowing it to be a free parameter in the fit did not significantly affect either the quality of the fit or the resulting value of k_C. The major removal processes for the dimer are flow out of the reactor with rate constant k_F and coagulation with monomer, reaction (7). Minor removal processes are deposition on the walls of the CSTR with rate constant k'_W, and coagulation with dimer and with larger particles

$$D + D \rightarrow P, \tag{11}$$

$$D + L \rightarrow P \tag{12}$$

and

$$D + P \rightarrow P \tag{13}$$

with rate constants k'_C. The rate equation for the dimer is

$$\frac{d[D]}{dt} = k_F[D]_0 + k_c[M]^2 - \{k_F + k'_w + 2k'_c([M] + [D] + [L] + [P])\}[D]. \tag{14}$$

To evaluate Eqs. (10) and (14) requires $[L]$ and $[P]$ as functions of time. The former is obtained from the measured number concentrations of the $2V$ peak. The latter are obtained from the rate equation

$$\frac{d[P]}{dt} = k_c\{2[M][D] + 2[M][L] + [D]^2 + 2[D][L] + [L]^2\} - \{k_F + k'_w\}[P]. \tag{15}$$

The rate equations were integrated numerically and the parameters were adjusted using non-linear least squares to provide the best fit to the data. $[M]_0$ and $[D]_0$ were assumed to change instantaneously between zero and constant values when the voltage on DMA#1 was turned on or off. Since the equations refer to concentration in the CSTR, a small correction for coagulation in the sample lines downstream of the CSTR was made. This consisted of reducing $[M]$ by $2k_C M^2 \Delta t_2$ and increasing $[D]$ by $k_C M^2 \Delta t_2$ where Δt_2 is the time delay as defined in the procedure section. The uncertainties in the delay times, Δt_1 and Δt_2, lead to an uncertainty of 2.3% in the coagulation rate constants.

Four parameters (k_C, k_W, k'_W, $[M_0]$) were fit simultaneously. k_F was calculated from the reactor volume and flow rate; the fit is not sensitive to this parameter (maximum effect on k_C was 0.4%) since it always appears in combination with parameters that were fit. Also, k'_C was assumed to be equal to k_C. These two coagulation rate constants are expected to be very similar in magnitude since the size difference between the monomer and dimer is not very large. The fits were not sensitive to the value of k'_C; the expected difference of less than 13% between k_C and k'_C produces a change of less than 0.4% in the coagulation constant. In the fits, the initial rise in the concentrations was most sensitive to $[M]_0$ and $[D]_0$, the decays during flushing were most sensitive to k_W and k'_W, and the steady state was most sensitive to k_C.

In some cases, the monomer number density slowly drifted upwards or downwards, occasionally by as much as 4% per hour during the steady-state period of the experiment. For those data where drifting was observed, the input number concentration, $[M]_0$ was allowed to be linear function of time; this added another parameter to the fit.

Based on the scatter of data about the fitted lines, the standard deviations of the fitted values of k_C were typically 2–5%. As noted above, the estimated uncertainties in input monomer and dimer concentration amounted to 7.4%. However, in some cases the disagreement between the sum of the peaks measured with DMA#2 and the total number was substantially greater than this error. In those cases, the uncertainty in the number concentrations was taken as the difference between the two methods of determining the total. Errors in other inputs to the fit contribute an uncertainty of 2.4%. These three sources of uncertainty were combined in quadrature to obtain estimates of the uncertainties in the measured rate constants. The percentage uncertainties averaged 13% and ranged from 7.6 to 37%. Identifiable sources of systematic error are substantially smaller than these random errors.

4. Results and discussion

The coagulation rate constants resulting from this work are plotted in Fig. 5. The error bars are one sigma uncertainties estimated as described above. Also shown are the rate constants for equal

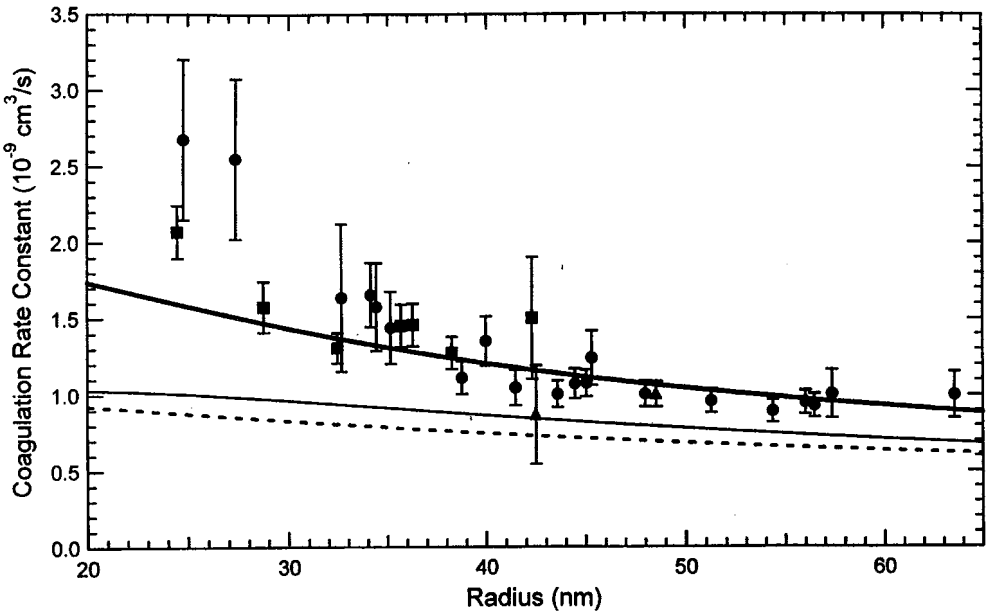

Fig. 5. Size dependence of the coagulation rate constants. Thin solid line is the value calculated from Sceats hard sphere collision theory. The bottom dotted line is the value calculated from Fuchs hard sphere collision theory. The thick solid line is the best-fit result for the experimental data ($A = 16kT$). The error bars are the estimated one sigma uncertainties for each data point. Circles, squares, and triangles represent 72.5, 72.2, and 71.7 wt% H_2SO_4, respectively.

size particles calculated using the hard sphere collision theories of Sceats (1989) and of Fuchs (1964) and the rate constants calculated accounting for van der Waals' forces calculated as discussed below. The experimental results show enhancements relative to the hard sphere rate constants ranging from 1.2 for the largest particles (127 nm) to 2.8 for the smallest particles (49 nm). These are comparable to the factor of two enhancement reported by McMurry (1980) for H_2O–H_2SO_4 particles with diameters of 20–50 nm and the enhancement factors of 1.2–2.0 reported by Van Dingenen and Raes (1990) for H_2O–H_2SO_4 aerosols with diameters of 200–30 nm. Before we attribute this enhancement to van der Waals' forces, we must eliminate the possibility that the results are artificially high due to either incomplete mixing or turbulent coagulation.

4.1. Wall losses, mixing, and turbulent coagulation

These three processes are all driven by turbulence and so are closely linked. The coagulation rate constants will be erroneously high if the turbulence is too weak to produce complete mixing or so strong that coagulation is enhanced by velocity shear in the gas. The wall loss rate constants are obtained from the experiments and provide a means to get some insight into the degree of turbulence in the reactor. It should be noted that the wall loss rate constants are highly uncertain since they depend on the difference between the CSTR flushing rate and the observed decay rate of the aerosol concentration. This difference is typically about 10–25%; as a result the wall loss rate constants are very sensitive to variations in the flow rate through the CSTR.

For particles in the size range used in these experiments, the wall loss rate constants should be almost entirely determined by diffusion. We have corrected the wall loss rate constants by subtracting the sedimentation rate constants calculated using

$$k_{sed} = 3U_{sed}/4R, \tag{16}$$

where U_{sed} is the sedimentation velocity and R is the radius of the CSTR. This correction amounts to no more than 5%. The resulting wall loss rate constants are plotted as a function of Brownian diffusion coefficient in Fig. 6. Fitting the results to a power law of the form

$$k_{wall} - k_{sed} = AD_B^n \tag{17}$$

yields $n = 0.71 \pm 0.13$, in excellent agreement with the value of 0.75 predicted by the theory of Landau and Levich (Fuchs, 1964). When applied to a sphere of radius R, this theory gives

$$k_{wall} - k_{sed} = (U^*/2R)(D_B/\nu)^{0.75}, \tag{18}$$

where U^* is friction velocity and ν is the kinematic viscosity of the gas. Fixing the exponent in Eq. (17) as 0.75 yields $A = 2.10 \pm 0.13$ $cm^{-1.5}$ $s^{-0.25}$. Since the CSTR has a radius of about 11 cm, Eq. (18) yields a friction velocity of approximately $10\,cm\,s^{-1}$.

With this result we can roughly estimate the time scale for macroscale mixing in the reactor by turbulent diffusion. The eddy diffusion coefficient, D_E, as a function of distance z from the wall is given by (Fuchs, 1964)

$$D_E \approx 0.3U^*z. \tag{19}$$

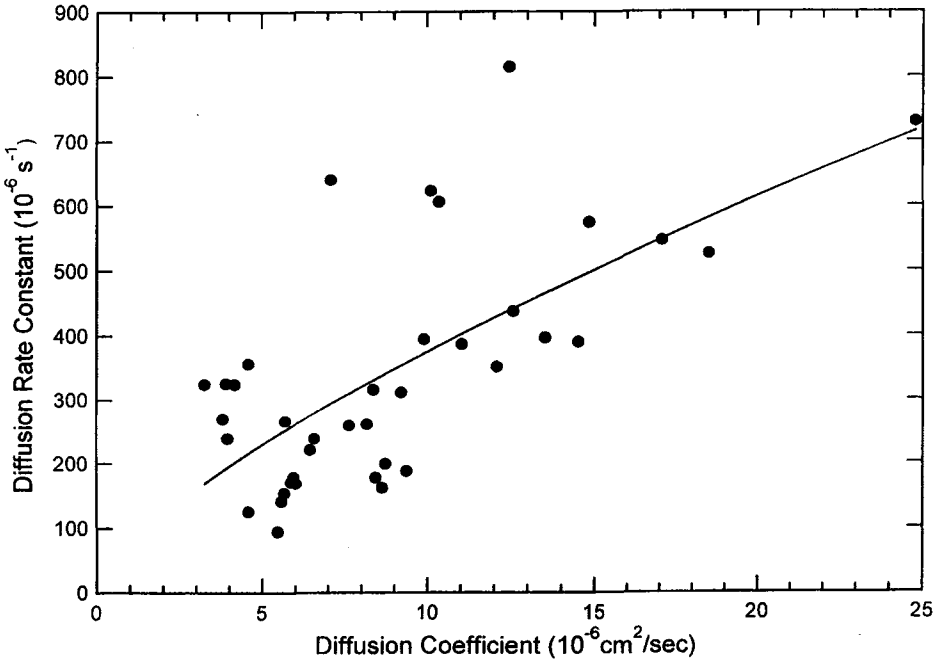

Fig. 6. Wall loss rate constants, corrected for sedimentation, as a function of particle diffusion coefficient. The line is the best fit to a simple power law.

This will not apply all the way to the center of the reactor. Evaluating this at $z = R/2$ yields $D_E = 17\,cm^2\,s^{-1}$; the average over the volume of the CSTR will be somewhat smaller than this since lower values will apply near the walls and at the center. The time constant for diffusional mixing in a sphere is (Crank, 1975, Section 6.3.6) $R^2/(4.5D_E) = 1.5$ s. A more realistic value may be two or three times as large. This value is considerably smaller than the CSTR residence time of 650 s and is consistent with the observation, reported above, that the mixing is sufficient to suppress concentration fluctuations during the filling and flushing of the CSTR.

The coagulation rate constants are determined mainly by the data obtained at steady state. Then the maximum fractional error due to insufficient mixing should be of the order of the fractional difference in the steady-state concentration of monomer and the concentration in the flow entering the CSTR; call this fractional error E_0. For these experiments, E_0 is in the range 0.05–0.09. As the fluid resides in the CSTR, mixing reduces the variations in concentration. If the fractional error, E, decays exponentially with time constant t_M and if the residence time in the CSTR is t_R, then we have

$$E = E_0 \exp(-t_R/t_M). \tag{20}$$

Since $t_R = 650$ s, the error will be negligible if t_M is in the order of 100 s or less.

The mixing time constant, t_M, must include both the time constant for macroscale mixing by eddy diffusion, estimated above, and the time constant for microscale mixing by diffusion. The later time constant is of the order of magnitude given by (Pohorecki & Baldyga, 1983)

$$t_{\text{microscale}} \approx (\nu/\varepsilon)^{1/2}(D_B/\nu), \tag{21}$$

where ε is the rate of energy dissipation per unit mass of fluid. This can be estimated by (Pond, Stewart & Burling, 1963)

$$\varepsilon \approx (2.5U^{*3})/R. \tag{22}$$

Using the friction velocity estimated above, we obtain $\varepsilon = 230\,cm^2\,s^{-3}$ and micromixing time constants in the range of 0.2–0.3 s for the range of Brownian diffusion coefficients encountered in these experiments. These estimates are based on the assumption of fully isotropic, homogeneous turbulence. This will not apply through the fluid, in particular it cannot apply near the walls. Even allowing for this and for the fact that there appears to be considerable uncertainty over the expression for the exact value of this time constant, it is clear that it is sufficiently short to ensure complete mixing in these experiments.

Excessive turbulence can have the effect of enhancing coagulation. There are two aspects of this that must be considered. One of these is inertial effects resulting from the fact that the particles are constantly subjected to accelerations of the fluid. For the present experiments, these effects should be negligible since the relaxation times of the particles are of the order of 10^{-7} s while the Kolmogorov time scale of the fluctuations, given by $(\nu/\varepsilon)^{1/2}$ (McComb, 1991), is of the order of 0.025 s. Thus, we expect that the particles should closely follow the fluid flow.

The second way in which turbulence can enhance coagulation is via turbulent enhancement of the diffusion coefficient. According to Williams (1988), the multiplicative enhancement factor g is

$$g = \frac{1}{[1 - (\pi x/2) + x\tan^{-1}x]}, \tag{23}$$

where

$$x = 2a(0.15/D_B)^{1/2}(\varepsilon/\nu)^{1/4}. \tag{24}$$

For the largest particles, with $a = 64$ nm and $D_B = 4.6 \times 10^{-6}$ cm^2 s^{-1}, this yields $g = 1.023$, the factor decreases to $g = 1.004$ for the smallest particles. Thus, if the value used for the energy dissipation rate is not an over estimate, the rate constants measured for the largest particles may be slightly larger than the actual values.

4.2. Determination of the Hamaker constant

The rate constants as a function of particle size were fit to theory to determine the Hamaker constant. The most widely used theory for calculating coagulation rate constants is the hard sphere theory of Fuchs (1964). This theory was not designed to incorporate interparticle forces and its generalization (Marlow, 1980) to account for the effect of interparticle forces in the transition regime is very complex. The theory of Sceats (1989) was derived specifically for the case of interparticle interactions and gives a much simpler formula for the transition regime; it also gives very similar hard sphere results to the Fuchs theory (see Fig. 5). Because of its convenience and appropriateness to the problem at hand, we use the theory of Sceats here. The calculations describe the interparticle force in terms of the Hamaker constant; this constant mainly depends on the composition of the particles. Reliable values of the Hamaker constant for H_2SO_4–H_2O particles are not available.

In the formulation of Sceats (1989), the coagulation rate constant for the kinetic and diffusion limited regimes are given by

$$k_K = (\tfrac{\pi}{2})(a_i + a_j)^2 c_{ij} E(\infty) \tag{25}$$

and

$$k_D = 2\pi(a_i + a_j) D_{ij} E(0), \tag{26}$$

where a_i and a_j are the radii of the particles, c_{ij} as the mean relative speed of the particles, D_{ij} is the relative diffusion coefficient (i.e., the sum of the diffusion coefficients of the two particles), and $E(\infty)$ and $E(0)$ are the enhancement factors for Knudsen numbers of infinity and zero, respectively. In terms of these limits, the transition regime coagulation rate constant is given by

$$k_T = k_K(\sqrt{1 + t_{ij}^2} - t_{ij}), \tag{27}$$

where

$$t_{ij} = \frac{k_K}{2k_D}. \tag{28}$$

To determine the enhancement factors, the expressions given by Sceats (1989) were solved numerically for values of the reduced Hamaker constant, A', ranging from 0.01 to 1000. These expressions ignore the effect of retardation on the interparticle interaction. The calculated enhancement factors were fit to within 0.8% by the expressions

$$E(0) = 1 + a_1 x + a_3 x^3 \tag{29}$$

and

$$E(\infty) = 1 + \frac{\sqrt{A'/3}}{1 + b_0\sqrt{A'}} + b_1 x + b_3 x^3, \tag{30}$$

where x is $\ln(1 + A')$, $a_1 = 0.0757$, $a_3 = 0.0015$, $b_0 = 0.0151$, $b_1 = -0.186$ and $b_3 = -0.0163$. The numerator in the second term in Eq. (30) was chosen to give the analytically derived limiting behavior at small values of A'. The reduced Hamaker constant is related to the Hamaker constant, A, via

$$A' = \frac{A}{kT}\frac{4a_i a_j}{(a_i + a_j)^2}. \tag{31}$$

The above equations, with $a_i = a_j$, were used in a weighted non-linear regression routine to find the value of the Hamaker constant that best fit the measured rate constants. In this fit, the results of experiments in which filling and flushing was done separately were not used. The data were weighted using the uncertainties for each measured rate constant. The best fit, shown by the heavy line in Fig. 5, corresponded to $A' = 16 \pm 6$ or $A = (6.4 \pm 2.6) \times 10^{-13}$ erg; the uncertainties are 95% confidence limits. The fit is consistent with the estimated uncertainties as determined by the value of the chi-square probability (Press, Flannery, Teukolsy & Vettering, 1989, Chapter 14). The uncertainties in A and A' are large because k_C has only a logarithmic dependence on the Hamaker constant; the corresponding uncertainties in calculated rate constants are only 4–5%. The Hamaker constant obtained here is in good agreement with the value of 5.4×10^{-13} erg estimated by McMurry (1980).

The residuals in this fit show a small but statistically significant trend indicating that, as the diameter decreases, the rate constant increases more strongly than predicted by the theory. We cannot say if this is real or if it is due to a slight systematic error in the experiments. If the trend is real, it may to do to the approximate nature of the theory used here. There was no observable effect of the slight variation in composition examined here.

As noted above, there was occasionally poor agreement between the total particle concentration determined from the size distribution and the total measured by CNC#1. If it is assumed that the later number is correct, and that the error is uniform over the small range of sizes in the distribution, then the rate constants can be adjusted by using the ratio of the two totals. When this was done, the fit was improved slightly and gave $A' = 12 \pm 5$; this agrees with the previous determination within the error limits. Since we do not understand the origin of the discrepancy between the concentration measurements, we do not think that it is appropriate to prefer this adjusted value.

Finally, we consider the possible effect of retarded interactions; the theory used here does not account for this. When the particles are far enough apart that the finite speed of light must be taken into account, the enhancement due to the intermolecular attraction will go down significantly. An approximate distance beyond which the retarded interaction of particle needs to be considered is given by Schmidt-Ott and Burtscher (1982). This distance depends on the particle size and the Hamaker constant. We calculated an upper limit to the effect of retardation for a Hamaker constant of 22 kT, using the largest particle size employed in this work (about 127 nm). A simple upper limit was obtained by assuming that the intermolecular attraction drops to zero once the

shortest distance between the two particles is beyond the transition distance given by

$$d_T = \frac{3hC}{8\pi^2 A}. \tag{32}$$

(Schmidt-Ott & Burtscher, 1982); this certainly gives an over estimate of the effect of retardation. The result of this calculation showed that for $A = 22\,kT$, the upper limit for the effect of retarded interactions was less than 1%. We therefore conclude that the neglect of retarded interactions is justified.

5. Conclusion

We have developed a tandem differential mobility analyzer method for measuring coagulation rate constants that uses the rate of formation of the coagulation products rather than the rate of change of the total number concentration or the growth of a particle size distribution. This method provides a useful means for obtaining coagulation rate constants as a function of particle size for equal size particles. For uncharged H_2SO_4/H_2O particles (72.5% H_2SO_4 by weight) at 298 K with diameters ranging from 49 to 127 nm, we observed an enhancement factors ranging from 1.2 to 2.8 relative to the values calculated for sticky hard spheres using the method of Sceats (1989). The larger enhancement factors were obtained for the smaller particles. The results are in reasonable agreement with the approximate theory of Sceats with van der Waals forces taken into account. The best-fit value of the Hamaker constant was found to be $(6.4 \pm 2.6)10^{-13}$ erg. This constant gives enhancement factors of 1.30–1.58 over the measured diameter range. Using Eqs. (29) and (30), the enhancement factor is found to be 1.25 in the diffusion (continuum) limit and 2.27 in the kinetic (free molecule) limit.

Acknowledgements

We thank Richard Leaitch of the Atmospheric Environment Service for the loan of a condensation nucleus counter. Funding was provided by the Natural Sciences and Engineering Research Council of Canada.

References

Alam, M. K. (1987). The effect of van der Waals and viscous forces on aerosol coagulation. *Aerosol Science and Technology, 6*, 41.

Brockmann, J. E., McMurry, P. H., & Liu, B. Y. H. (1982). Experimental study of simultaneous coagulation and diffusional loss of free molecule aerosols in turbulent pipe flow. *Journal of Colloid and Interface Science, 88*, 522.

Crank, J. (1975). *The mathematics of diffusion.* (2nd Ed). Oxford: Clarendon Press.

Fuchs, N. A. (1964). *The mechanics of aerosols.*. Oxford: Pergamon Press.

Fuchs, N. A., & Stugin, A. G. (1965). Coagulation rate of highly dispersed aerosols. *Journal of Colloid Science, 20*, 492.

Gmitro, J. I., & Vermeulen, T. (1964). Vapor–liquid equilibria for aqueous sulfuric acid. *American Institute of Chemical Engineering Journal, 10*, 740.

Huang, D. D., Seinfeld, J. H., & Marlow, W. H. (1990). BGK equation solution of coagulation for large Knudsen number aerosols with a singular attractive contact potential. *Journal of Colloid and Interface Science, 140*, 258.

Knutson, E. O., & Whitby, K. T. (1975). Aerosol classification by electric mobility: Apparatus, theory, and applications. *Journal of Aerosol Science, 6*, 443.

Leaitch, W. R., Isaac, G. A., Strapp, J. W., Banic, C. M., & Wiebe, H. A. (1992). The relationship between cloud droplet number concentrations and anthropogenic pollution; Observations and climatic implications. *Journal of Geophysical Research, 97*, 2463.

Marlow, W. H. (1980). Derivation of Aerosol collision rates for singular attractive contact potentials. *Journal of Chemical. Physics, 73*, 6284.

McComb, W. D. (1991). *The physics of fluid turbulence.* Oxford: Oxford University Press.

McMurry, P. H. (1980). Photochemical aerosol formation from SO_2: A theoretical analysis of smog chamber data. *Journal of Colloid and Interface Science, 78*, 513.

Mercer, T. T., & Tillery, M. I. (1971). Coagulation rates of particles produced in air by thoron. *Journal of Colloid and Interface Science, 4*, 785.

Okuyama, K., Kousaka, Y., & Hayashi, K. (1984). Change in size distribution of ultrafine aerosol particles undergoing Brownian coagulation. *Journal of Colloid and Interface Science, 101*, 98.

Pohorecki, R., & Baldyga, J. (1983). New model of micromixing in chemical reactor. 1. General development and application to a tubular reactor. *Industrial and Engineering Chemistry Fundamentals, 22*, 392.

Pond, S., Stewart, R. W., & Burling, R. W. (1963). Turbulence spectra in the wind over waves. *Journal of the Atmospheric Sciences, 20*, 319.

Preining, O. (1991). Aerosol and climate — an overview. *Atmospheric Environment, 11*, 2443.

Press, W. H., Flannery, B. P., Teukolsy, S. A., & Vettering, W. T. (1989). *Numerical recipes in pascal.*. Cambridge: Cambridge University Press.

Pui, D. Y. H., & Kinney, P. D. (1991). Use of electrostatic classification method to size 0.1 mm SRM particles — a feasibility study. *Journal of Res. National Institute of Stand. Technology, 96*, 147.

Rader, D. J., & McMurry, P. H. (1986). Application of the tandem differential mobility analyzer to studies of droplet growth or evaporation. *Journal of Aerosol Science, 17*, 771.

Saxena, V. K., & Menon, S. (1999). Sulfate-induced cooling in the southeastern U.S.: An observational assessment. *Geophysical Research Letters, 16*, 2489.

Sceats, M. G. (1989). Brownian coagulation in aerosols — the role of long range forces. *Journal of Colloid and Interface Science, 129*, 105.

Schmidt-Ott, A., & Burtscher, H. (1982). The effect of van der Waals forces on aerosol coagulation. *Journal of Colloid and Interface Science, 89*, 353.

Schwartz, S. (1996). The whitehouse effect — shortwave radiative forcing of climate by anthropogenic aerosols: An overview. *Journal of Aerosol Science, 3*, 359.

Shon, S.-N., Kasper, G., & Shaw, D. T. (1980). An experimental study of Brownian coagulation in the transition regime. *Journal of Colloid and Interface Science, 73*, 233.

Stolzenburg, M. R., & McMurry, P. H. (1988). TDMAFIT users's manual, university of Minnesota Particle Technology Laboratory Publication No. 653.

Twomey, S. (1991). Aerosols, clouds and radiation. *Atmospheric Environment, 25A*, 2435.

Van Dingenen, R., & Raes, F. (1990). Coagulation enhancement of H_2O–H_2SO_4 aerosols: Experiments and model calculations in the transition regime. *Journal of Aerosol Science, 21*, s237.

Wang, S. C., & Flagan, R. C. (1990). Scanning electrical mobility spectrometer. *Aerosol Science and Technology, 13*, 230.

Wiedensohler, A. (1988). An approximation of the bipolar charge distribution for particles in the submicron size range. *Journal of Aerosol Science, 19*, 387.

Williams, M. M. R. (1988). A unified theory of aerosol coagulation. *Journal of Physics D, 21*, 875.